Stability of Biological Membranes upon Mechanical Indentation: Supplementary Information

Florian Franz,[†] Camilo Aponte-Santamaría,[‡,¶] Csaba Daday,[†] Vedran Miletić,[†] and Frauke Gräter[*,†,¶]

†*Molecular Biomechanics Group, Heidelberg Institute for Theoretical Studies, 69118 Heidelberg, Germany*

‡*Max Planck Tandem Group in Computing, University of Los Andes, 111711 Bogotá, Columbia*

¶*Interdisciplinary Center for Scientific Computing, 69120 Heidelberg, Germany*

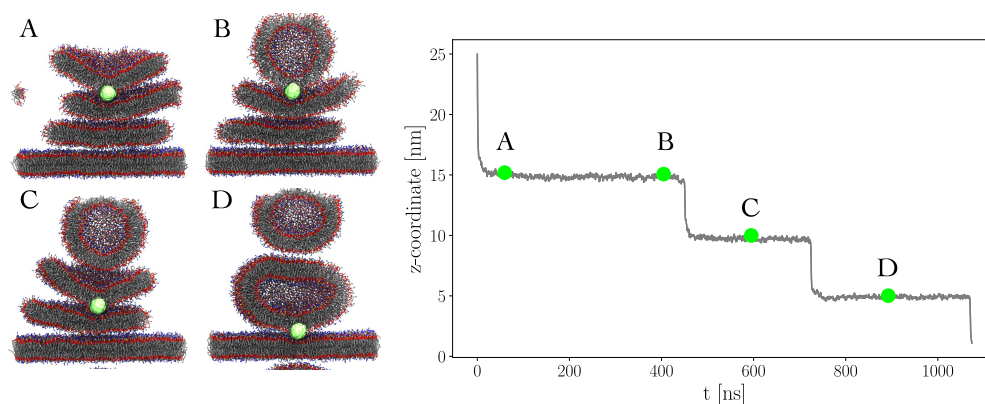E-mail: frauke.graeter@h-its.org

Phone: +49-6221-533267

Figure S1: **Coarse-grained multi-bilayer rupture process for a hydrophilic indenter sphere.** The hydrophilic indenter sphere is pulled along the negative z-direction. A trajectory is shown for a constant pulling force of $0.64\,\text{nN}$. The snapshots (*left*) illustrate the trajectory and the respective sphere positions are marked in the time evolution curve (*right*). For a hydrophilic sphere, dwelling regions lie at different z-positions. Also, vesicle formation is likely due to the small patch size.
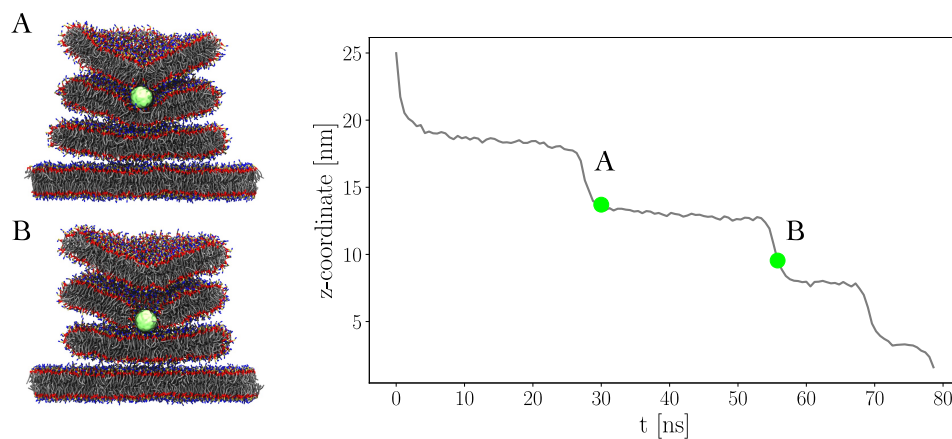

Figure S2: **Coarse-grained multi-bilayer rupture process for a hydrophobic indenter sphere.** The hydrophobic indenter sphere is pulled along the negative z-axis. Here, data is shown for a constant pulling-force of $0.58\,\text{nN}$. The snapshots (*left*) illustrate the trajectory, and the respective sphere positions are marked in the time evolution curve (*right*).
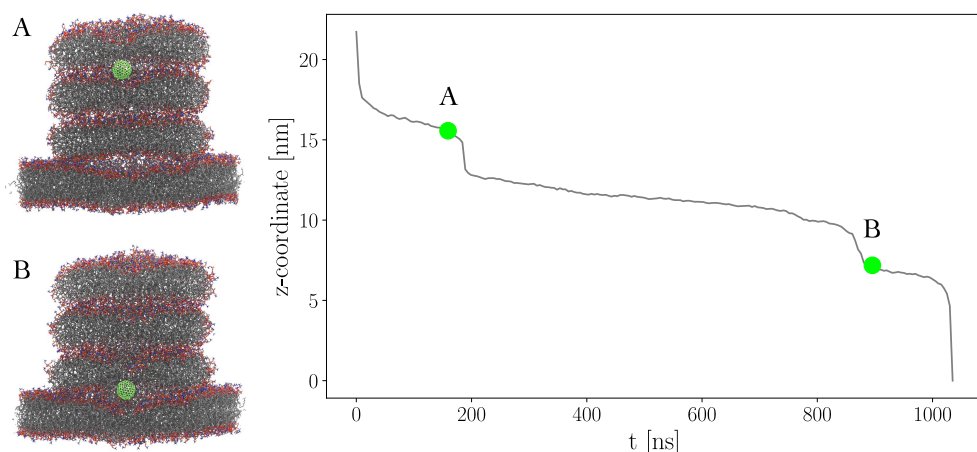
Figure S3: **Atomistic multi-bilayer rupture process.** The indenter sphere is pulled downwards along the z-axis. Here, data is shown for a constant force of $1.33\,\text{nN}$. The snapshots (*left*) depict the sphere right before rupturing the first double layer of head groups (A), and right after having passed through the second double layer of head groups (B). The respective sphere positions are marked in the time evolution curve (*right*). Steps in the vertical position of the indenter are again very evident, even though the plateaus are less stable due to the larger forces and shorter time scales.
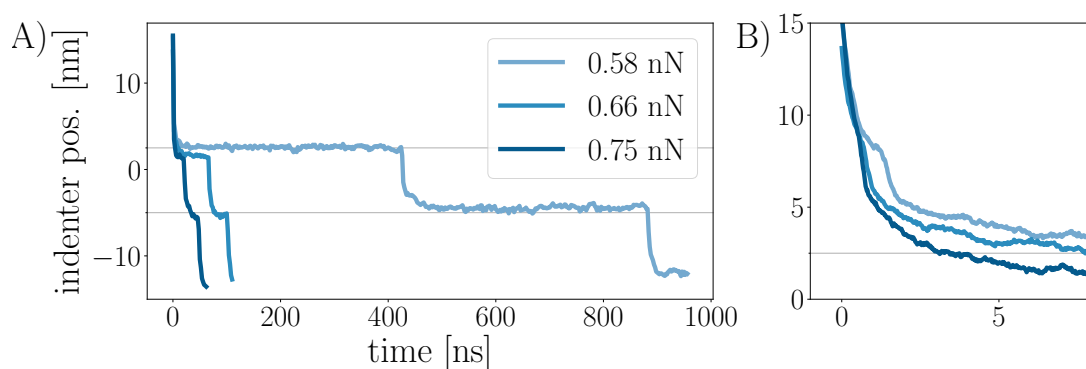

Figure S4: **Initial rupture of MBL with hydrophobic indententation** A) Indenter sphere position versus time curves. B) Zoom into the first $8\,\text{ns}$ of the sphere position shows small kinks associated with the rupture of the first head-group leaflet.
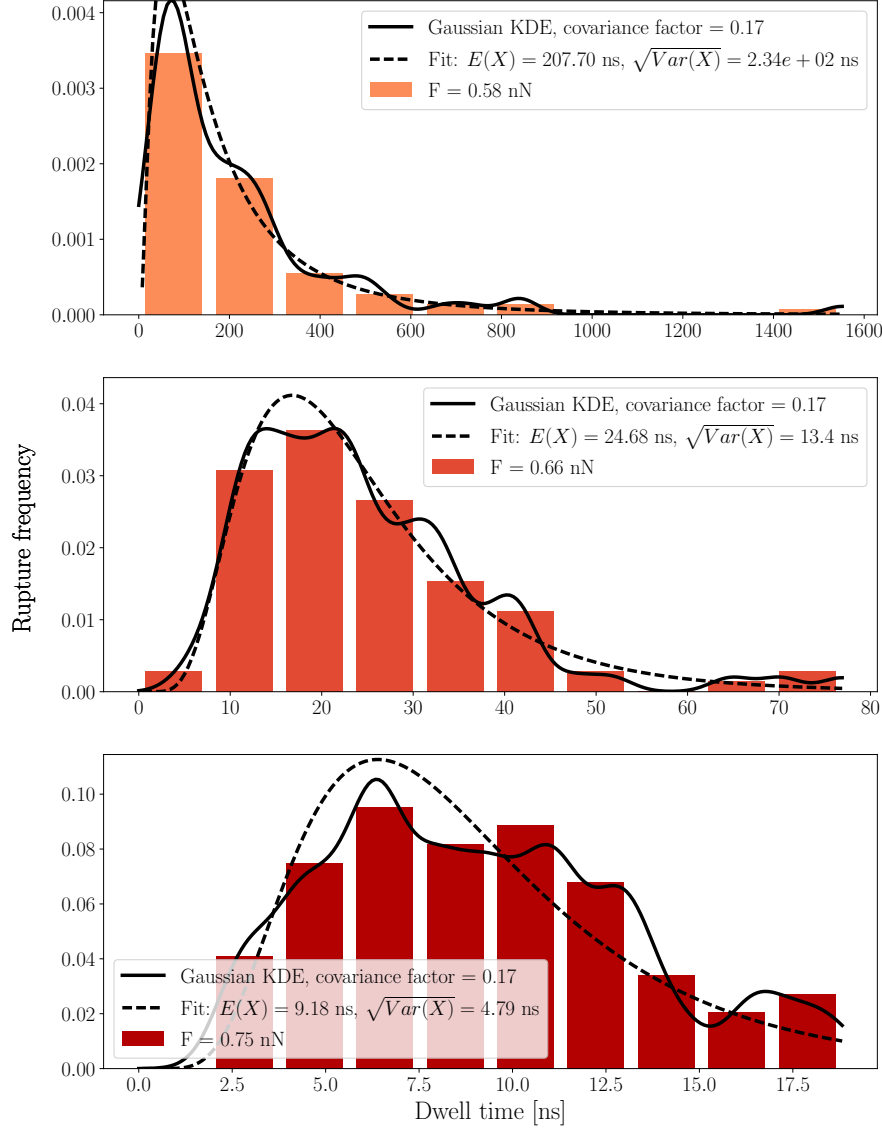
Figure S5: **Distribution of dwell times for MBL with hydrophilic indentation** Normalized histograms as well as a Gaussian kernel density estimate (KDE, black line) are shown for each data set. A log-normal distribution is fitted to the KDE. Goodness of fit from top to bottom: ($F = 0.58\,\mathrm{nN}$, $\alpha = 0.0678$, $P = 0.786$); ($F = 0.66\,\mathrm{nN}$, $\alpha = 0.0423$, $P = 0.996$); ($F = 0.75\,\mathrm{nN}$, $\alpha = 0.0741$, $P = 0.785$).
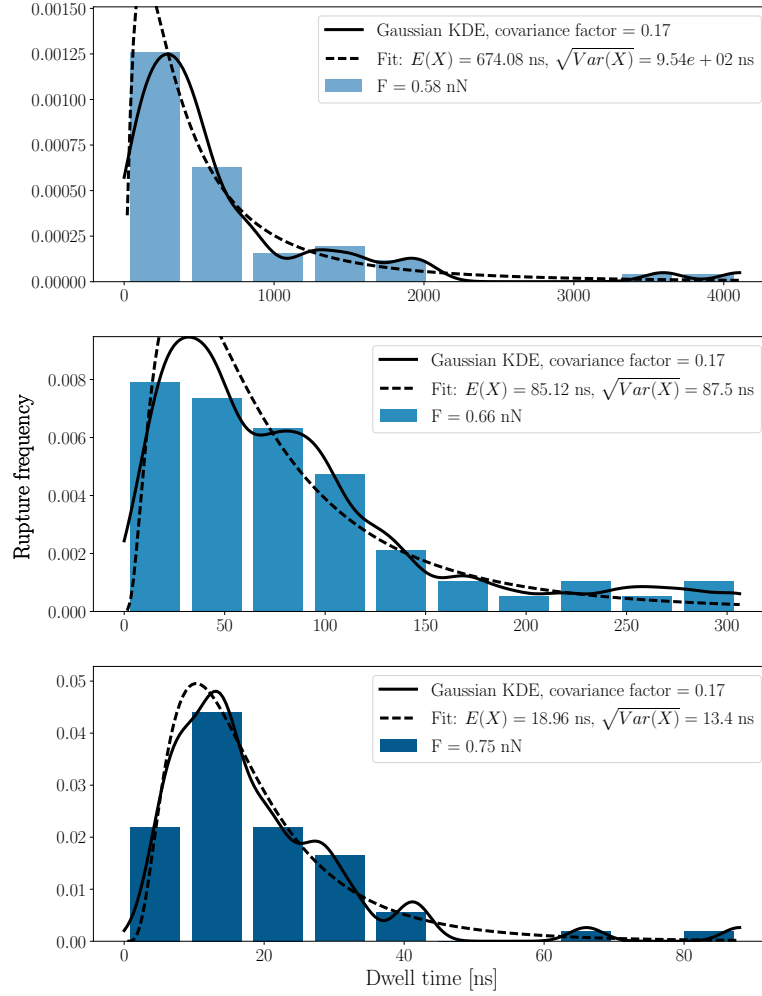
Figure S6: **Distribution of dwell times for MBL with hydrophobic indentation** Normalized histograms as well as a Gaussian kernel density estimate (KDE, black line) are shown for each data set. A log-normal distribution is fitted to the KDE. Goodness of fit from top to bottom: ($F = 0.58\,\mathrm{nN}$, $\alpha = 0.0845$, $P = 0.781$); ($F = 0.66\,\mathrm{nN}$, $\alpha = 0.0657$, $P = 0.951$); ($F = 0.75\,\mathrm{nN}$, $\alpha = 0.0545$, $P = 0.993$).
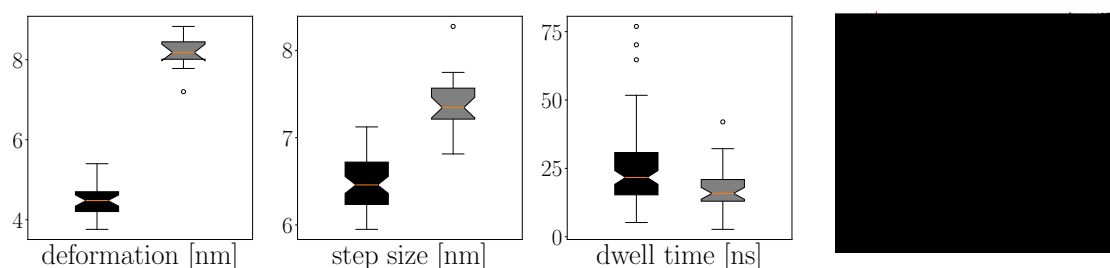
Figure S7: **Stacked system with increased membrane area and hydrophilic indenter** The data was obtained from a total of 33 rupture processes recorded for an indenting force of $0.66\,\text{nN}$. The boxplots compare vertical membrane deformation, step size, and dwell times of the big system (gray) to the reference system (black). The snapshot depicts the time frame used for the extraction of the deformation of the second layer (90% of the dwelltime passed).
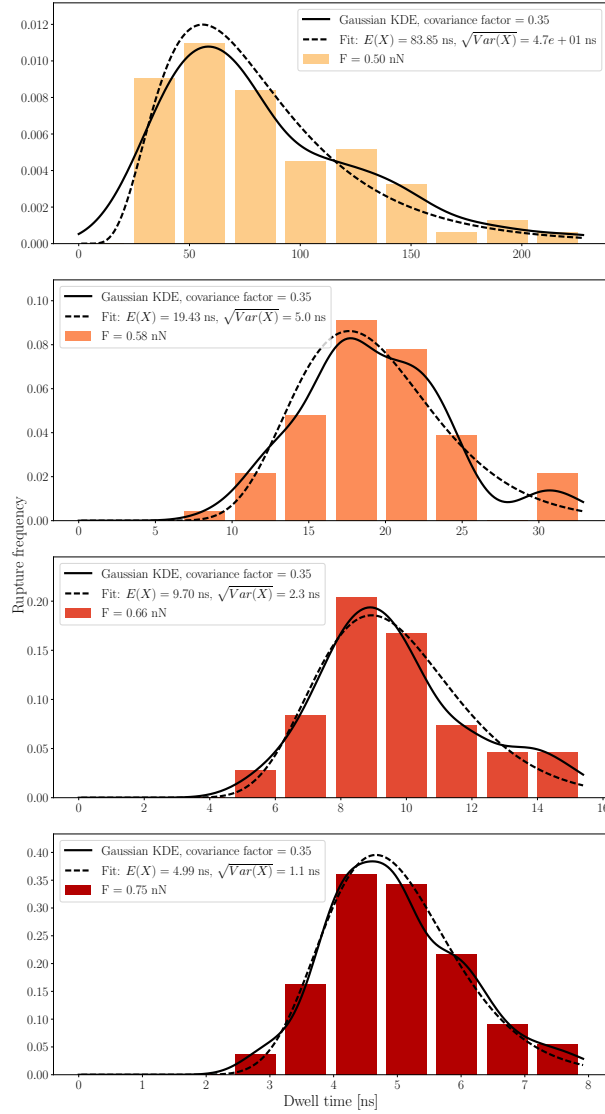
Figure S8: **Distribution of dwell times for SBL with hydrophilic indentation** Normalized histograms as well as a Gaussian kernel density estimate (KDE, black line) are shown for each data set. A log-normal distribution is fitted to the KDE. Goodness of fit from top to bottom: ($F = 0.50 \, \text{nN}$), $\alpha = 0.0602$, $P = 0.996$); ($F = 0.58 \, \text{nN}$, $\alpha = 0.0668$, $P = 0.913$); ($F = 0.66 \, \text{nN}$, $\alpha = 0.0665$, $P = 0.916$); ($F = 0.75 \, \text{nN}$, $\alpha = 0.0603$, $P = 0.960$).
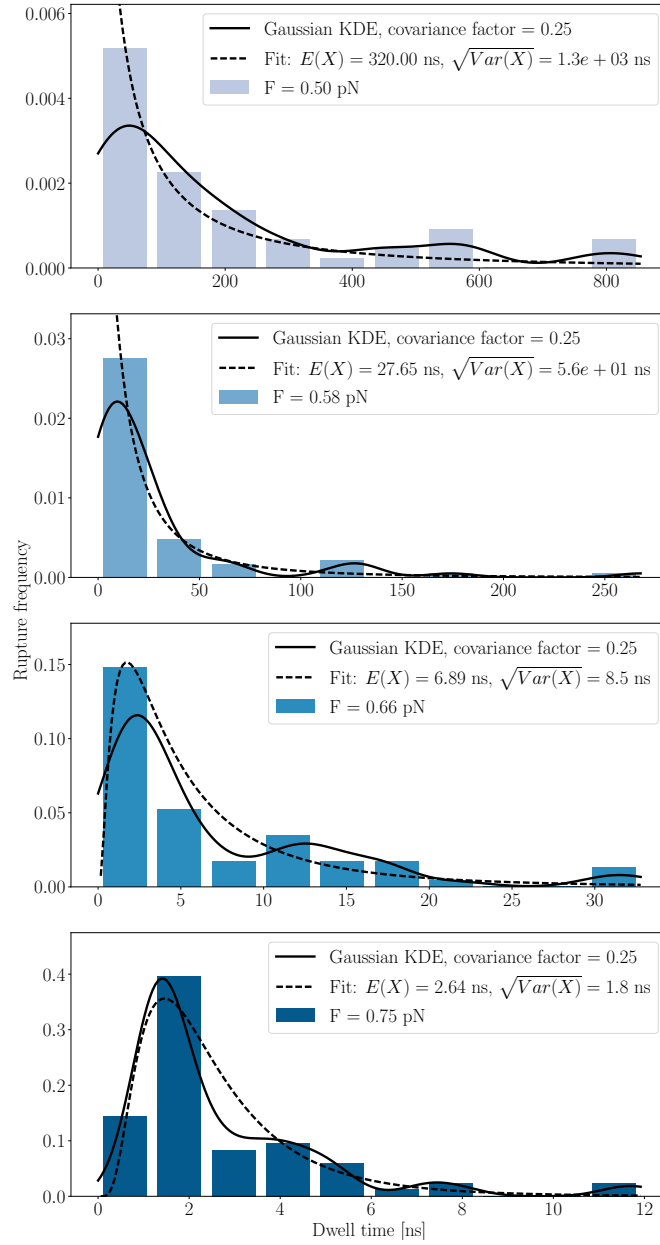
Figure S9: **Distribution of dwell times for SBL with hydrophilic indentation** Normalized histograms as well as a Gaussian kernel density estimate (KDE, black line) are shown for each data set. A log-normal distribution is fitted to the KDE. Goodness of fit from top to bottom: ($F = 0.50\,\text{nN}$, $\alpha = 0.0102$, $P = 0.638$); ($F = 0.58\,\text{nN}$, $\alpha = 0.0657$, $P = 0.927$); ($F = 0.66\,\text{nN}$, $\alpha = 0.1248$, $P = 0.207$); ($F = 0.75\,\text{nN}$, $\alpha = 0.1897$, $P = 0.111$)
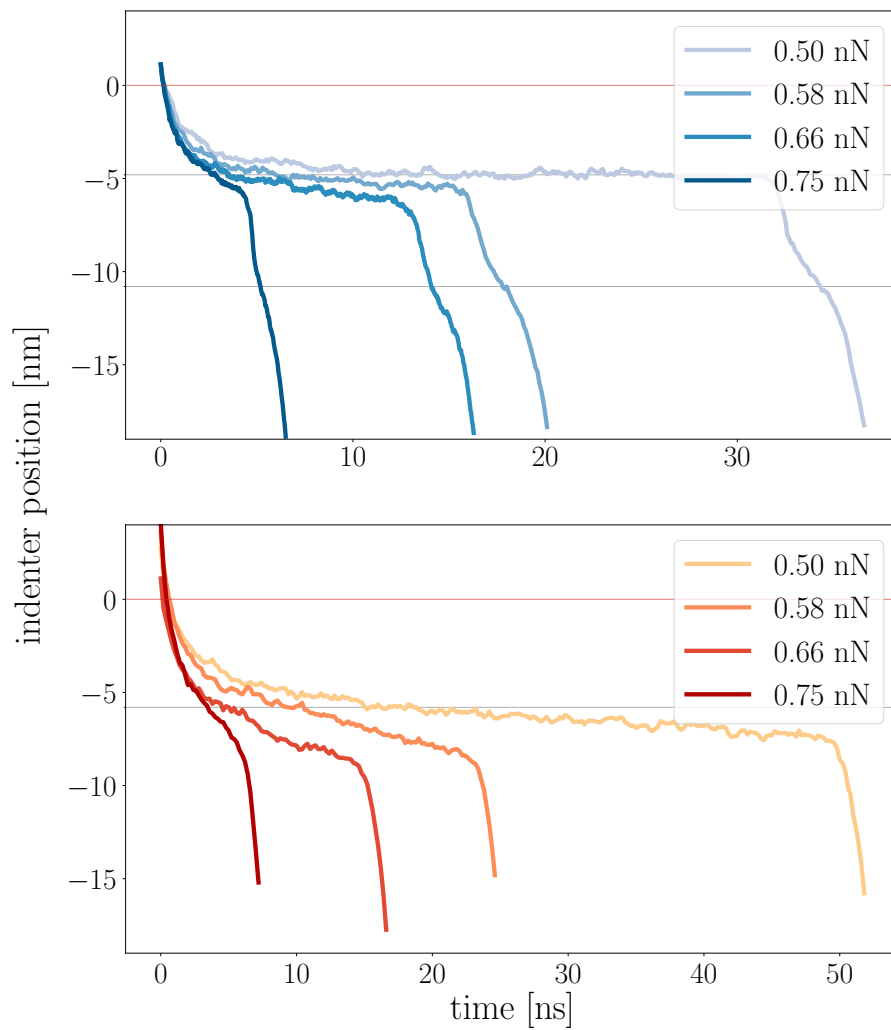
Figure S10: **Coarse-grained single-bilayer rupture process.** Indenter sphere position versus time curves for the rupture of single bilayers. For four forces ($F = 0.50\,\text{nN}$, $F = 0.58\,\text{nN}$, $F = 0.66\,\text{nN}$, and $F = 0.75\,\text{nN}$), we show one example rupture curve for the hydrophilic (*bottom*), and the hydrophobic (*top*) indenter. An indenter position of zero corresponds to the position of the first head-group layer before it makes contact with the sphere.
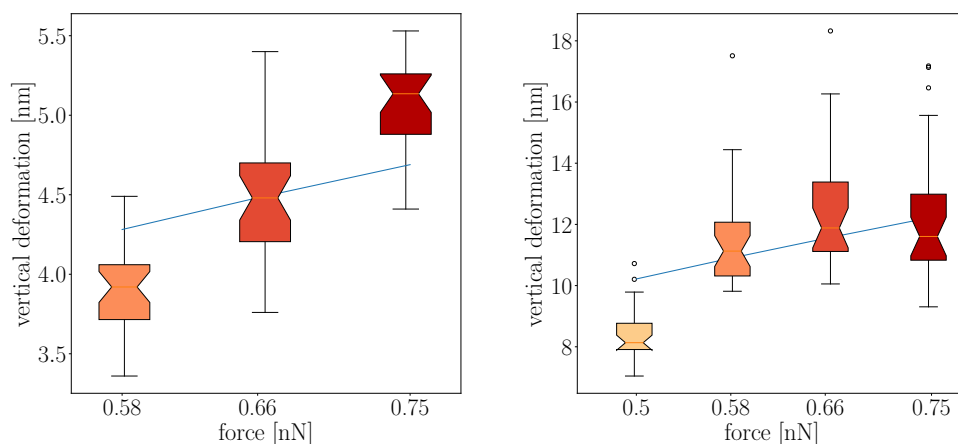
Figure S11: **Indentation-induced membrane deformation.** For coarse-grained membrane stacks (*left*) and single layers (*right*), the vertical deformation was extracted. The frame from which the deformation was calculated was taken at the point where 90% of the dwell time of the respective trajectory had passed. The data was fitted to the a simple model proposed by Fraxedas et al.:[1] $F = k \cdot \delta \cdot (1 - (1\sqrt{\delta^2 + b^2}))$ where δ is the deformation and b is half the size of the simulation box. For the stack and the single membranes, this results in stiffnesses $k = 2.47 \pm 0.07\,\mathrm{nN/nm}$ and $k = 0.20 \pm 0.01\,\mathrm{nN/nm}$, respectively.
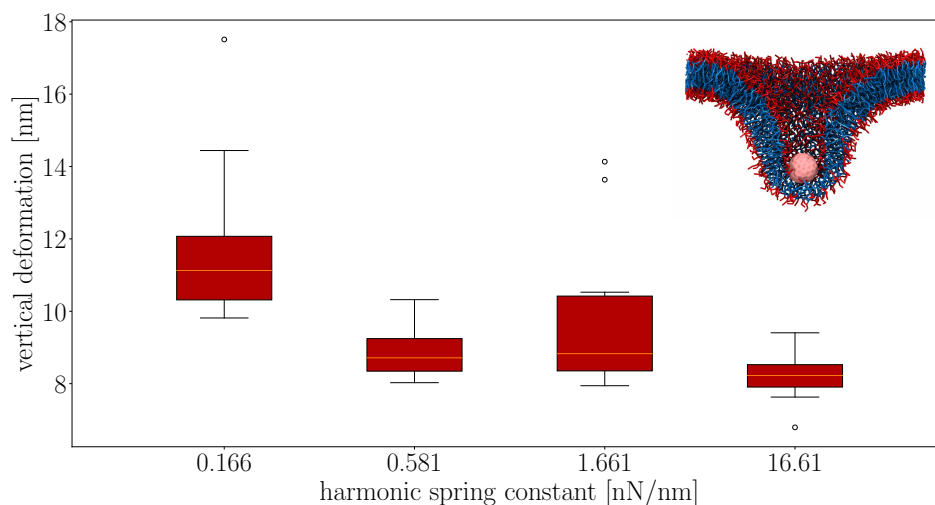

Figure S12: **Dependence of the membrane deformation on position restraints.** The deformation was extracted from at least 10 trajectories for each harmonic spring constant on the bilayer COM.
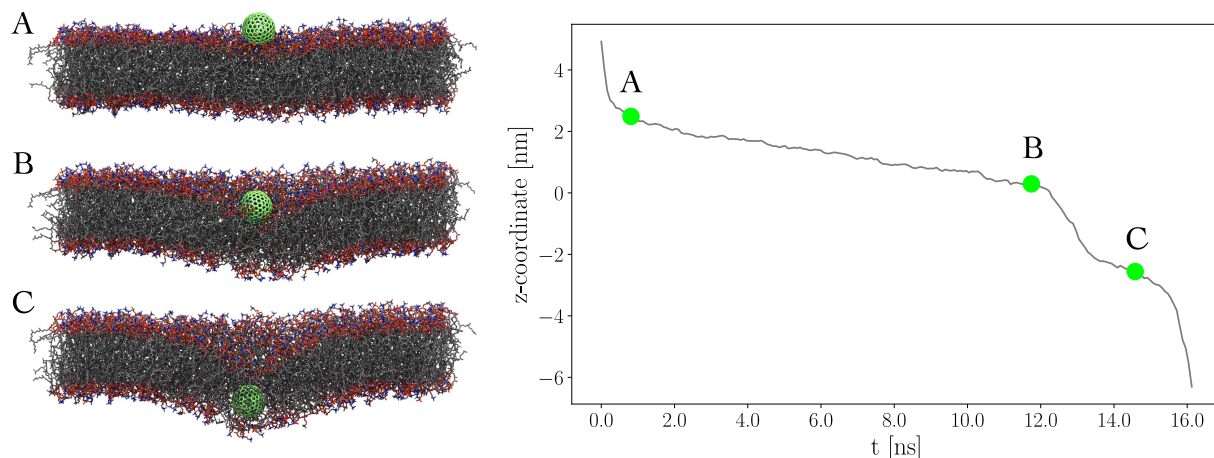
Figure S13: **All atom single-bilayer rupture process (hydrophobic indenter).** The indenter sphere is pulled along the z-axis. Here, data is shown for a constant force of $1\,\mathrm{nN}$. The snapshots (*left*) depict the sphere after it encounters the bilayer and starts dwelling at the top leaflet (A), right before it passes the upper layer of head-groups (B), and dwelling at the lower head-group layer (C). The respective sphere positions are marked in the time evolution curve (*right*).
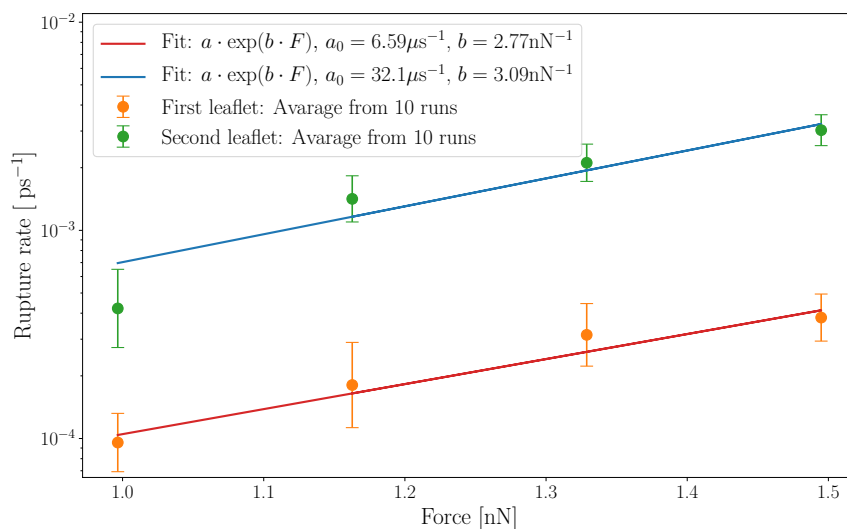

Figure S14: **All atom single-bilayer rupture rates versus force.** Average rupture rates are shown for each leaflet at four different forces between 1.00 and $1.49\,\mathrm{nN}$. For each leaflet the rupture rates can be fitted to an exponential function of the form $a\left(F\right) = a_0 \cdot \exp\left(F \cdot b\right)$ according to the Bell model.[2]
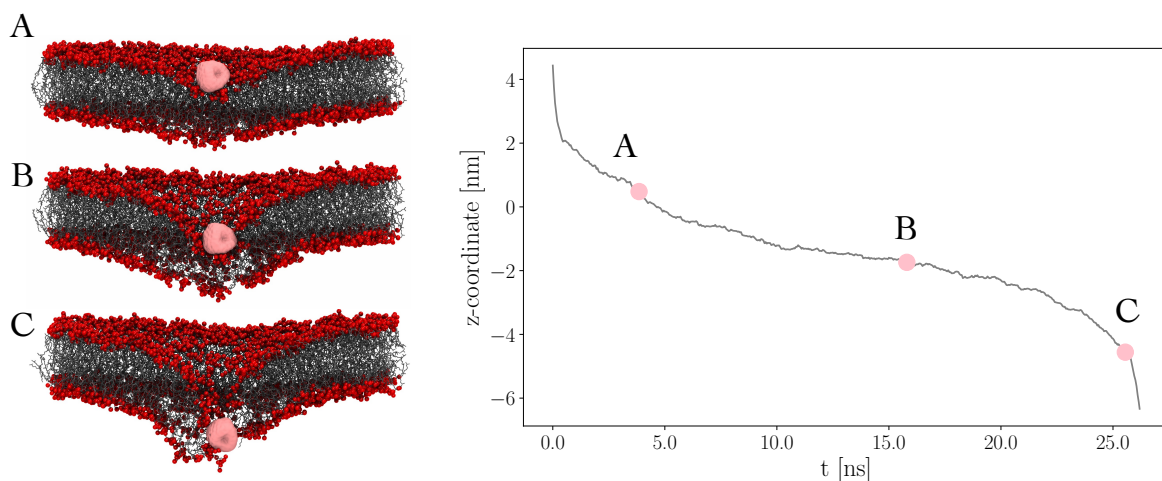
Figure S15: **All atom single-bilayer rupture process (hydrophilic indenter).** The indenter is pulled downward along the z-axis. Data is shown for a constant force of $1.5\,\mathrm{nN}$. The snapshots (*left*) depict the sphere during the process of dwelling (A,B) and at the point of rupture (C). Lipid head-group atoms are highlighted as red spheres. The respective indenter positions are marked in the time evolution curve (*right*).

References

(1) Fraxedas, J.; Garcia-Manyes, S.; Gorostiza, P.; Sanz, F. Nanoindentation: toward the sensing of atomic interactions. *Proc. Natl. Acad. Sci. U. S. A.* **2002**, *99*, 5228–5232.

(2) Bell, G. I. Models for the specific adhesion of cells to cells. *Science* **1978**, *200*, 618.